Enantioseparation via EIC-OSN: Process Design and Improvement of Enantiomers Resolvability and Separation Performance

Issara Sereewatthanawut
Membrane Extraction Technology Ltd, Unit 25, Talina Centre, Bagleys' Lane, London, SW6 2BW, U.K.

Frederico Castelo Ferreira
Institute for Biotechnology and Bioengineering (IBB), Centre for Biological and Chemical Engineering, Instituto Superior Técnico, Lisboa, Portugal; and Dept. of Chemical Engineering and Chemical Technology, Imperial College London, U.K.

Nazlee F. Ghazali and Andrew G. Livingston
Dept. of Chemical Engineering and Chemical Technology, Imperial College London, SW7 2AZ, U.K.

DOI 10.1002/aic.12025
Published online September 28, 2009 in Wiley InterScience (www.interscience.wiley.com).

This article presents a mathematical model to assess and optimize the separation performance of an enantioselective inclusion complexation-organic solvent nanofiltration process. Enantiomer solubilities, feed concentrations, solvent compositions, permeate solvent volumes, and numbers of nanofiltrations were identified as key factors for process efficiency. The model was first tested by comparing calculated and experimental results for a nonoptimized process, and then, calculations were carried out to select the best operating conditions. An important finding was that the optimal configuration varied with the objective function selected, e.g., resolvability versus yield, with a boundary on product optical purity. The model also suggested that the process efficiency could benefit from diafiltration of the distomer and from the use of higher feed concentrations. However, the latter strategy would result in higher losses of eutomer. To address this drawback, a multistage process was evaluated using the verified process model. © 2009 American Institute of Chemical Engineers *AIChE J,* 56: 893–904, 2010
Keywords: chiral resolution, enantioselective inclusion complexation, organic solvent nanofiltration, resolvability, membrane separation

Introduction

Preparation of enantiomerically enriched compounds for use in the agrichemical, food, and pharmaceutical industries is essential to obtain the desirable biological activity of racemic of products while avoiding adverse side effects. Isolation from the chiral pool, asymmetric synthesis, and chiral resolution are established methodologies to obtain pure enantiomers.[1] Diastereomeric resolution is one of the more robust resolution techniques, which employ relatively inexpensive resolving agents and, therefore, is commonly used at a large scale; however, it is restricted to the enantioseparation of acids and bases.[2] On the other hand, enantioselective inclusion complexation (EIC) uses more sophisticated chiral hosts, but allows the resolution of neutral molecules, such as alcohols, without the need for derivatization into an acid.

Correspondence concerning this article should be addressed to A. G. Livingston at a.livingston@imperial.ac.uk
Current address of Nazlee F. Ghazali, Dept. of Bioprocess Engineering, Faculty of Chemical and Natural Resources Engineering, Universiti Teknologi Malaysia, 81310 UTM Skudai, Johor, Malaysia

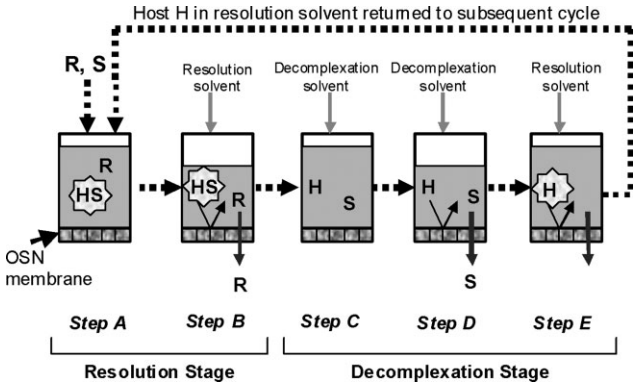

Figure 1. Schematic diagram of EIC-OSN process structure.

R and S represent (*R*)- and (*S*)-enantiomer (guest) while H represents chiral host.

Toda[3] used TADDOLs, a new family of chiral hosts for EIC resolutions, derived from inexpensive hydroxyl acids such as tartaric or lactic acid. Several authors recently reviewed and reported the use of TADDOLs as powerful resolving agents.[4,5] High chiral enantioselectivity between these hosts and a broad range of resolution substrates was observed, expanding the potential for practical EIC applications. However, in studies performed by Toda's research group, the recovery of the isolated enantiomers from the inclusion complex was performed by high vacuum distillation. This procedure limits EIC resolutions to compounds with a certain degree of volatility and requires the use of high vacuum and high distillation temperatures. In addition, the distillation of purified enantiomer from the postresolution slurry can hinder further scaling up due to mass and heat transfer limitations.

Several membrane-based processes have been proposed for chiral resolutions.[6] Over the past decades, nanofiltration has been successfully extended from aqueous systems to organic solvent systems, because new membranes compatible with solvents are developed.[7,8] Our research group recently reported a novel enantioseparation process, coupling the EIC technique with an organic solvent nanofiltration (OSN) separation.[9] The EIC-OSN process described below can be operated at room temperature, with a high to moderate yield and optical purity of products. The simplicity of the process and of the equipment required, together with the reusability of the host compounds, enhances the potential feasibility of this technique for pilot and industrial scale operations. This work presents a mathematical model that calculates the separation performance of the EIC-OSN process, which can, therefore, be used for the selection of process-operating conditions configuration. The model was tested against experimental data, which were obtained using racemic phenylethanol (*rac*-PET; 122 g/mol) as a guest species and (*4R,5R*)-(-)-2,2-dimethyl-α,α,α′,α′-tetraphenyl-1,3-dioxolane-4,5-dimethanol ((*R,R*)-TADDOL; 467 g/mol) as a chiral host.

Process description

The EIC-OSN process (Figure 1) involves two stages: a resolution and a decomplexation stage, each employing a different solvent. The resolution solvent promotes the selective recognition between solid host and the desired enantiomer (eutomer), resulting in the formation of a crystalline inclusion complex and leaving the undesired enantiomer (distomer) dissolved in solution. The decomplexation solvent ensures the dissociation of the complex in a homogeneous solution. A nanofiltration membrane compatible with both solvents is used in the first stage to elute the dissolved distomer out of the system and, in the second stage, to isolate the eutomer in the permeate solution and to retain the host for further use. In this study, the (*S*)-enantiomer is the eutomer, and the (*R*)-enantiomer is the distomer.

In Step A (Figure 1), racemic (eutomer and distomer) guest and chiral host are mixed at an equimolar ratio in the resolution solvent. The insoluble host recognizes and forms a crystalline inclusion complex with the eutomer, while the distomer remains dissolved. The mixture is stirred for 6 h, until it reaches equilibrium. In Step B, the resulting heterogeneous mixture is filtered and the inclusion complex is retained by the membrane, whilst the distomer leaves the process through the permeate solution. In Step C, decomplexation solvent is added to break the complex and obtain a homogenous solution in which host and eutomer are dissolved. In Step D, this solution is nanofiltered, and based on the differences between eutomer and chiral host molecular weights, it is possible to isolate the eutomer in the permeate solution, while the host is retained for further use. In Step E, the decomplexation solvent in the retentate is replaced by resolution solvent to allow Step A of the next cycle.

In this work, and in the previous feasibility study,[9] the different steps of this process were operated in successive batches. Within each of the filtration steps (B, D, and E), repeated nanofiltrations and varying feed volumes can be employed. The permeate stream of each step is the combined permeates of the nanofiltrations performed within that step. It was also previously established that *n*-hexane (or *n*-hexane/toluene mixtures up to a maximum concentration of 20% vol/vol of toluene in *n*-hexane) could effectively be used as a resolution solvent in Step A.[9] Therefore, in Step E, filtration number and volume must provide a resolution solvent composition of less than 20% vol/vol toluene for use in the next operation cycle. Complete dissolution of the complex is obtained in *n*-hexane/toluene mixtures with toluene concentrations higher than 60% vol/vol, and so any solvent mixture with >60% vol/vol toluene can effectively be used as a decomplexation solvent in Steps C and D. In this study, we optimized the volumes and number of filtrations used in Steps B and D (the (*R*)- and (*S*)-elution stages, respectively), because these variables determine the amounts of distomer ((*R*)-enantiomer) and eutomer ((*S*)-enantiomer), which are obtained in the permeate solutions and, consequently, the process yield and optical purity of the enantiomer-enriched products.

Process modeling and development

Model Assumptions and Boundaries. The model developed calculates the composition of (*R*)- and (*S*)-enantiomers in the permeate streams of the EIC-OSN process based on mass balances, solubility of inclusion complex, and membrane rejection to enantiomers and the host molecule. The

model was used to calculate the amount of each enantiomer and optical purity in permeate during filtration, and it was based on the following assumptions:

(a) Membrane rejection of the enantiomers is 0%.

(b) Membrane rejection of the host and inclusion complex is 100%.

(c) At operating feed concentration, only one enantiomer (the eutomer) complexes with the chiral host to form an inclusion complex, the uncomplexed enantiomer (the distomer) remains dissolved in the liquid.

(d) Ideal-solution behavior for liquid phase ($\gamma_i^l = 1$) is observed, and above saturation limit, the concentration of inclusion complex dissolved in the resolution solvent remains constant.

Because of the size of the nanofiltration equipment, we were limited experimentally to maximum filtration feed volumes of 300 cm^3 and minimum retentate volumes of 10 cm^3. Therefore, to facilitate experimental testing of the mathematical model, the feed and retentate volumes used as model parameters were kept within these limits, and when feed volumes and the number of filtrations in Steps B and D were parameters for optimization, the following volumes were fixed:

(a) The retentate volume of every filtration was fixed to the minimum value of 10 cm^3.

(b) When successive filtrations were performed within the same step, the volume of fresh solvent added to the retentate to make up the total feed volume of a given nanofiltration was equal to the permeate volume of the previous filtration (i.e., $V_{F,n} = V_{P,n-1}$).

(c) The volume of resolution solvent employed in Step A was fixed at 40 cm^3.

(d) In Step C, 30 cm^3 fixed volume of toluene was added to 10 cm^3 of resolution solvent (carried in from Step B), resulting in a homogeneous solution with a toluene concentration higher than 75% vol/vol toluene (well above the 60% vol/vol toluene required for total dissolution of the inclusion complex).

(e) In Step E, 30 cm^3 of *n*-hexane was added to 10 cm^3 of the decomplexation solvent (carried in from Step C and D), and the resulting 40 cm^3 feed volume was filtered until 10 cm^3 retentate remained. To this 10 cm^3 of solution, a further 30 cm^3 of *n*-hexane was added, ensuring a solvent composition in Step A suitable for resolution of about 6.2% vol/vol toluene in *n*-hexane, which was well below the maximum limit established at a value of 20% vol/vol.

Process Modeling. The efficiency of the process was evaluated using the yield and optical purity of the desired product, which was expressed in terms of enantiomeric excess (ee) and Fogassy's resolvability (*S*). The latter was introduced by Fogassy et al.[10] for quantitative evaluation of optical resolution. Note that in this study, we used ee and *S* as defined by Fogassy et al. However, we expressed yield differently. Fogassy et al.'s yield was the percentage of the total amount of enantiomers fed to the resolution that ended up in the resolution product, not discriminating between the enantiomers forms; here we used two independent yields, one for each enantiomer as defined below:

$$Y_n^R = \frac{M_n^R}{M_o^R} \times 100\% \quad for\ n = 1, 2, 3, \ldots \tag{1}$$

$$ee_n^R = \frac{M_n^R - M_n^S}{M_n^R + M_n^S} \times 100\% \quad for\ n = 1, 2, 3, \ldots \tag{2}$$

$$S_n^R = \frac{M_n^R - M_n^S}{0.5 M_o} \times 100\% \quad for\ n = 1, 2, 3, \ldots \tag{3}$$

$$Y_n^S = \frac{M_n^S}{M_o^S} \times 100\% \quad for\ n = 1, 2, 3, \ldots \tag{4}$$

$$ee_n^S = \frac{M_n^S - M_n^R}{M_n^S + M_n^R} \times 100\% \quad for\ n = 1, 2, 3, \ldots \tag{5}$$

$$S_n^S = \frac{M_n^S - M_n^R}{0.5 M_o} \times 100\% \quad for\ n = 1, 2, 3, \ldots \tag{6}$$

where Y_n^R and Y_n^S are the (*R*)- and (*S*)-enantiomer yield of permeate from nanofiltration *n*; ee_n^R and ee_n^S are the ee of (*R*)- and (*S*)-enantiomer corresponding to yield at nanofiltration *n*; S_n^R and S_n^S are resolvability of (*R*)- and (*S*)-enantiomer at step *n*, respectively; M_n^R and M_n^S are the number of moles of distomer ((*R*)-enantiomer) and eutomer ((*S*)-enantiomer) in the permeate of filtration *n*; M_o^R and M_o^S are the initial moles of distomer and eutomer fed to the cycle; M_o is the initial moles of racemate fed to a given cycle; and *n* is the filtration number.

The model is based on two mechanisms: dilution and dissolution.

For uncomplexed (*R*)-enantiomer, the distomer remains dissolved throughout the entire process. As solvent is fed to the process and filtrations performed, the distomer is diluted in both resolution and decomplexation stages. Hence, the mol of distomer obtained in permeate from each filtration can be calculated as follows:

$$M_n^R = \begin{cases} \frac{V_{P,n}}{V_{F,n}} M_o^R & for\ n = 1 \quad (7) \\ \frac{V_{P,n}}{V_{F,n}} \left(M_o^R - \sum_{i=1}^{n-1} M_i^R \right) & for\ n = 2, 3, 4, \ldots \quad (8) \end{cases}$$

where $V_{P,n}$ is the volume of permeate from filtration *n*; and $V_{F,n}$ is the initial volume of feed at nanofiltration *n*.

The eutomer forms an inclusion complex with the solid host during the resolution (Step A). This complex has a low solubility limit in the resolution solvent, and therefore the larger part of the eutomer is present at equilibrium as a crystalline solid, while a smaller fraction remains dissolved, saturating the solution. As long as the system is at saturation conditions (i.e., crystalline inclusion complex is present), the concentration of eutomer dissolved remains constant. Because additional resolution solvent is added in Step B, more eutomer will dissociate from the complex to maintain the solution saturated in free eutomer, and when this solution is nanofiltered, a fraction of the eutomer is carried out in the permeate. Therefore, the dissolution mechanism is considered for the eutomer during the successive filtrations taking place in Step B, and the mol of eutomer in permeate of each nanofiltration *n* can be calculated as follows:

$$M_n^S = V_{P,n} K_s \quad for\ n = 1, 2, 3, \ldots, d \tag{9}$$

where K_S is the saturation concentration of the eutomer (i.e., (*S*)-enantiomer) in the liquid (which is at equilibrium with the solid inclusion complex); and *d* is the last nanofiltration number of Step B of a particular cycle.

During the decomplexation (Step C), decomplexation solvent is added to ensure that the inclusion complex fully

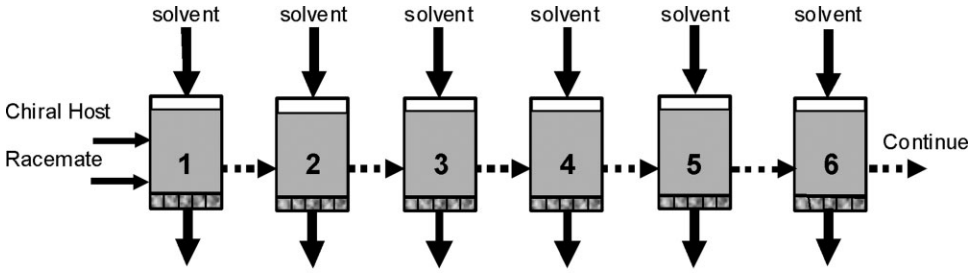

Configuration Description		
Configuration	Stage/Solvent	
	Resolution ((*R*)-elution)	Decomplexation ((*S*)-elution)
I	1	2-6
II	1-2	3-6
III	1-3	4-6
IV	1-4	5-6
V	1-5	6

Figure 2. EIC-OSN alteration for solvent addition.

For example, Configuration I, volume 1 of added solvent is resolution solvent, volumes 2-6 of added solvent are decomplexation solvent, etc.

dissociates and that all the eutomer dissolved in a homogeneous solution. Therefore, over the nanofiltrations carried out in Step D, and further addition of decomplexation solvent, the dilution mechanism applies, and the moles of eutomer obtained in the permeate from each nanofiltration of Step D can be calculated as follows:

$$M_n^S = \frac{V_{P,n}}{V_{F,n}}\left(M_o^S - \sum_{i=1}^{n-1} M_i^S\right) \quad for\ n = d+1,\ d+2,\ d+3, \ldots \tag{10}$$

Optimization Rational. The optimal conditions of this process were determined by two interrelated approaches, namely "distribution of nanofiltrations approach" and "feed volume selection approach."

Approach 1: Distribution of nanofiltrations. In this approach, the free variable is the number of nanofiltrations performed within each filtration Steps B and D. Initially, the total volumes of added solvent for these two steps were fixed at six. Thus, five configurations were arranged as illustrated in Figure 2, Configuration I-V. The volume of resolution solvent increased from I to V, whilst the volume of decomplexation solvent decreased from V to I.

Approach 2: Feed volume selection. Different feed volumes of resolution and decomplexation solvents can be used in nanofiltration Steps B and D. Therefore, Approach 1 was applied for several feed solvent volumes simultaneously to determine the optimal condition; gPROMS simulation package version 2.3 (Process System Enterprise Ltd., UK) was used to find the optimal value of resolvability (S^s) of the desired product. The program used the sequential quadratic programming method for solution of the nonlinear optimization. This method used a quadratic model and a linear model for the objective function and the constraint, respectively.

The two approaches were applied simultaneously using the same objective function. Yield and ee are the important outputs of this process, which combined as resolvability. Therefore, the objective function is eutomer resolvability in permeate from Step D (i.e., (*S*)-elution stage):

$$\begin{aligned} \max \quad & S_D^S = \frac{\sum_{i=d+1}^{6} M_i^S - \sum_{i=d+1}^{6} M_i^R}{0.5 M_o} \times 100\% \\ & \left(Over\ Configuration\ I \rightarrow V\ and\ V_{P,2/3/4/5/6}0 \rightarrow 300\right) \\ s.t. \quad & Eqs.\ 7, 8, 10 \\ & V_{P,1} = 30 \\ & V_{P,n} \geq 15 \qquad for\ n = d+1,\ d+2,\ d+3,\ \ldots, 6 \end{aligned} \tag{11}$$

Experimental

Solubility profiles

The solubilities (K_S and K_R) of the two enantiomers after inclusion complex formation in the resolution solvent are key parameters for the model and, therefore, must be determined. In this work, three secondary alcohols and one amine were selected for solubility measurements: *rac*-PET (122 g/mol; Sigma-Aldrich), *rac*-phenylpropagyl alcohol (132 g/mol; Sigma-Aldrich), *rac*-phenylpropanol (136 g/mol; Fluka), and *rac*-phenylethylamine (PEA; 121 g/mol; Sigma-Aldrich). The solubilities of these compounds were measured in pure *n*-hexane at concentrations from 25 mol/m^3 to 400 mol/m^3 after being mixed with equimolar amounts of (*R,R*)-TADDOL (467 g/mol; Sigma-Aldrich) in 4 cm^3 of *n*-hexane (Fisher Scientific, UK). The solutions obtained were stirred at room temperature in a reaction carousel tube (RDT, UK) for 6 h, then the suspension was allowed to settle, and 1.5 cm^3 of solution was centrifuged (Micro Contour, MSE, UK) for 15 min. The centrifuged solution was then analyzed by GC (Agilent) using an HP-CHIRAL-20β column (Agilent). Following the above protocol, the solubility of *rac*-PET at 50 mol/m^3 after complexation with equimolar amounts of (*R,R*)-TADDOL were also measured in 6.2%

vol/vol, 12.8% vol/vol, and 14.4% vol/vol toluene in *n*-hexane solutions.

Model verification

To test the model, a given number of EIC-OSN cycles were carried out. The *rac*-PET and (*R,R*)-TADDOL were selected as guest and host, respectively. HPLC grade *n*-hexane and toluene (Fisher Scientific, UK) were used as resolution solvent and decomplexation solvent, respectively. A polyimide membrane, STARMEM^{TM}122* (kindly supplied by Membrane Extraction Technology, UK) with a molecular weight cut off† of 220 g/mol was placed at the bottom of a stainless steel nanofiltration vessel (SEPA ST Cell; Osmonics), with an effective membrane area of 13.9 cm^2. After preconditioning the membrane by filtering 450 cm^3 of toluene at 3 MPa, 0.922 g of (*R,R*)-TADDOL (1.976 mmol) and 0.250 g of *rac*-PET (2.044 mmol) were mixed in *n*-hexane (40 cm^3) in the cell. The mixture was stirred at room temperature for 6 h (Step A), and 3 MPa pressure was then applied using N_2 gas to filter the solution (Step B). When 30 cm^3 of permeate was collected, the cell was depressurized, and 30 cm^3 of *n*-hexane was then added to the 10 cm^3 retentate to perform the next filtration. Three filtrations with identical volumes of feed and permeate collected were performed within Step B. Subsequently, 30 cm^3 of pure toluene was added to decomplex the inclusion complex (Step C). Again, 3 MPa pressure was applied until 30 cm^3 of permeate was collected (Step D), then 30 cm^3 of additional toluene was added to the retentate to perform the next filtration. A total of three nanofiltrations were performed within Step D. Following this last filtration, 30 cm^3 of pure *n*-hexane was added to the 10 cm^3 retentate to exchange the (*R,R*)-TADDOL into resolution solvent for the next cycle (Step E); the resulting 40 cm^3 was nanofiltered, and further 30 cm^3 of *n*-hexane was added to the 10 cm^3 of retentate, ensuring that the resulting 40 cm^3 solution sent to Step A of the next cycle had a toluene concentration of about 6.2% vol/vol, well below the required 20% vol/vol.

Two cycles were conducted for the purpose of model verification, however, the second cycle differed from the first one, because (i) there was no further addition of (*R,R*)-TADDOL in Step A; and (ii) 30 cm^3 of 15% vol/vol toluene in *n*-hexane solution was added at the end of the first and second nanofiltrations of Step B instead of pure *n*-hexane. Therefore, the toluene concentrations in *n*-hexane were 6.2%, 12.8%, and 14.4% vol/vol for the first, second, and third filtrations, respectively, of Step B of the second cycle.

After using the model to select optimal configuration and volumes, an additional cycle was experimentally performed using calculated volumes for each filtration according to the selected configuration.

Results and Discussion

Solubility profiles

Figure 3 shows the concentrations of (*R*)- and (*S*)-enantiomers that remained dissolved in *n*-hexane after a 6-h resolution with equimolar amounts of (*R,R*)-TADDOL. Different initial concentrations of racemic secondary alcohols and an amine were used as substrates. These solubility profiles control the efficiency of the resolution process (Step A). In an ideal scenario, the entire amount of distomer added would remain completely dissolved in solution, and the concentration of eutomer in solution would be zero (Figure 3a, dashed line).

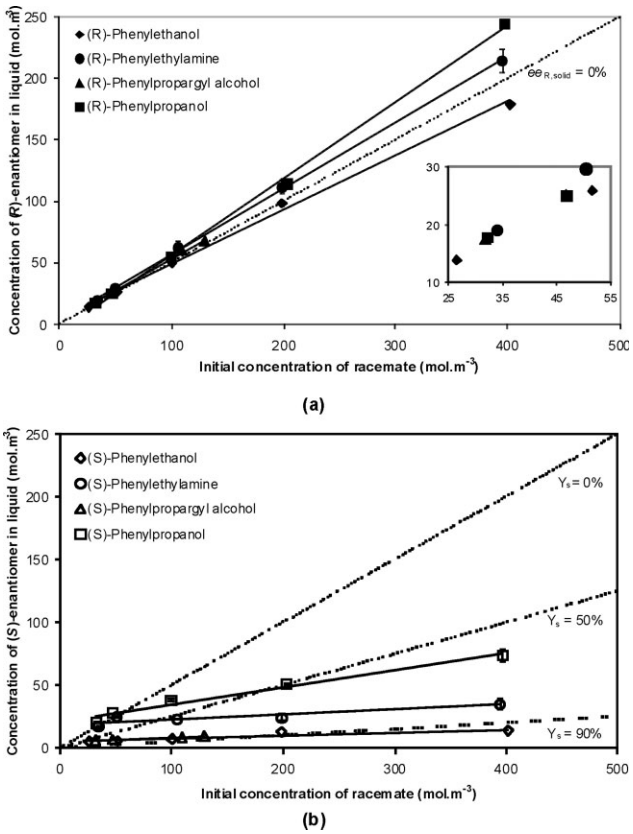

Figure 3. Solubility profiles of secondary alcohols and amine enantiomers in *n*-hexane after formation of inclusion complex for feed concentrations from 25 mol/m^3 to 400 mol/m^3.

Equimolar TADDOL was used for 6-h resolution. For *rac*-phenylpropargyl alcohol, saturated concentration at room temperature is 130.6 mol/m^3 in *n*-hexane.

When a fraction of the fed distomer binds with the host, the fraction of distomer that remains dissolved in solution is lower, and the experimental values reported in Figure 3a fall below the dashed line. The results from Figure 3a indicate that the distomer remained entirely dissolved in the resolution solvent up to 400 mol/m^3 of added racemate for all substrates except phenylpropargyl alcohol. For PET, some of the distomer seemed to be bound to the host. For the other substrates, the final concentration of distomer in resolution solvent was slightly higher than the initial concentration (values above dashed line). This can be explained by the evaporation of the resolution solvent, *n*-hexane, because the tested concentration was considerably high (400 mol/m^3 in 4 cm^3), a small amount of evaporated solvent could significantly change the concentration.

*STARMEM is a trademark of W.R. Grace & Co., USA.

†Molecular weight cut off (MWCO) is defined by the interpolation from a curve of rejection versus molecular weight as the molecular weight corresponding to 90% rejection.

Figure 3b shows the concentration of eutomer remaining in solution. The best case scenario corresponds to the total absence of eutomer from solution, implying its complete complexation and, therefore, a resolution yield (Y^S) of 100%; the worst case scenario happens when all the eutomer remains dissolved in solution and no resolution occurs. Unfortunately, the best case scenario did not occur, because a fraction of the eutomer had to remain in solution to balance equilibrium toward the formation of the enantiomeric-inclusion complex. The data show that for all the racemates tested, resolution yields (Y^S) higher than 50% were achievable, while for PET they can reach values of about 90%. Step B was carried out to provide an efficient elution of the distomer. However, some of the eutomer was also eluted in this step, which was then compensated by dissolution of the inclusion complex to maintain the saturation equilibrium, leading to lower eutomer yields in Step D. This is the basis of the dissolution mechanism. The eutomer solubility limits obtained in *n*-hexane indicate that the solubility was concentration dependent. In addition, these limits were specific of the solvents or solvent mixtures used. For example, at a feed concentration of 50 mol/m^3 of *rac*-PET and equimolar (*R*,*R*)-TADDOL, the respective (*S*)-enantiomer solubility was 5.7 mol/m^3 in pure *n*-hexane, but it increased to 6.0, 9.0, and 9.4 mol/m^3 for solutions of 6.2%, 12.8%, and 14.4% vol/vol of toluene in *n*-hexane, respectively. The solubility limits, as a function of enantiomer concentrations and solvent composition, were used as inputs for the process simulations.

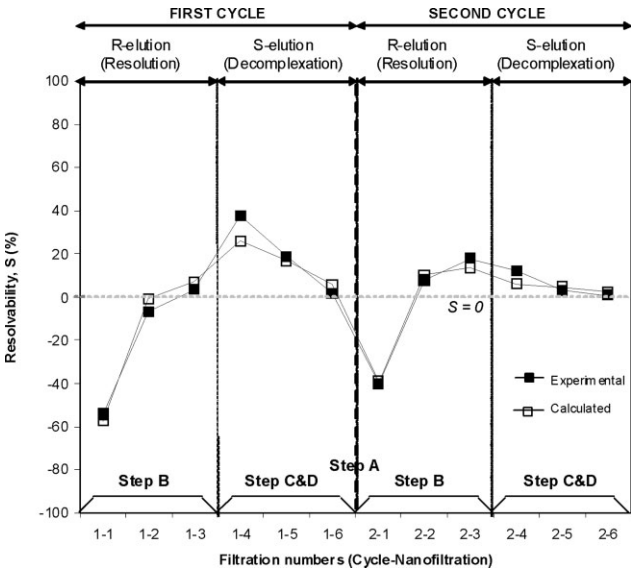

Figure 4. Experimental and calculated profiles of resolvability of (*S*)-PET for the six nanofiltration permeates.

rac-PET at 50 mol/m^3 was employed as substrate. Feed solvent volumes were fixed at 40 cm^3, corresponding to 30 cm^3 of the permeate volumes. Positive *S* indicates (*S*)-rich permeate.

Comparison between calculated results and experimental data

The same *rac*-PET concentration of 50 mol/m^3 used in the previous feasibility study[9] was used. At this concentration, the (*R*)-PET remained entirely soluble, and at saturation conditions (i.e., some solids are present), the concentration of (*S*)-PET remained constant at 5.7 mol/m^3 in pure *n*-hexane. To test the model, calculations and experiments were carried out as described in the experimental section for two operation cycles, using Configuration III (see Figure 2) and 40 cm^3 of feed solvent (corresponding to a permeate volume of 30 cm^3) for each of the six nanofiltrations performed in Steps B and D.

Figure 4 compares the experimental with the calculated results for (*S*)-enantiomer resolvability (S^S) in each of the six nanofiltrations. Overall, good agreement was achieved between experimental data and calculated results for both cycles, with an *R*-squared value of 0.961. Therefore, we considered this model suitable for process optimization. The differences between calculated and experimental resolvability could be attributed to oscillations of membrane rejections to (*R*)- and (*S*)-enantiomers due to membrane compaction, fouling, variations in solution viscosity, or solvent evaporation.

Negative S^S indicates that permeate from the resolution mainly contains (*R*)-PET. The experimental and calculated results showed the same trend, in which S^S was at the minimum value at the first nanofiltration of resolution stage (Step B), corresponding to an elution of the dissolved (*R*)-PET. In the second and third filtration, S^S increased toward positive values, because less (*R*)-PET remained in the system, and additional (*S*)-PET was dissolved and eluted. In the decomplexation stage (Step D), S^S was at the maximum value at the first nanofiltration and decreased in the following nanofiltrations, because there was less (*S*)-PET eluted in the permeate. As expected, negative S^S was found in Step B (resolution stage), where the (*R*)-enantiomer was mainly eluted, whereas S^S positive values appeared in Step D (decomplexation stage), where the majority of (*S*)-PET was obtained. Specifically, in the first cycle, the S^S of the combined permeate stream was −51.67% for Step B ((*R*)-elution stage) and 48.16% for Step D ((*S*)-elution stage).

As highlighted in the experimental section, Step B of the second cycle was not performed with pure *n*-hexane, but with increasing amounts (6.2%, 12.8%, and 14.4% vol/vol) of toluene dissolved in *n*-hexane for each of the first three filtrations. Therefore, instead of the constant K_S of 5.7 mol/m^3 used as a model input in the first cycle, three different measured K_S values at 6.0, 9.0, and 9.4 mol/m^3 were used as model inputs for the first, second, and third filtrations of the second cycle respectively. This procedure aims to test the sensitivity of the process and model to the presence of toluene during the resolution stage. Again, in the second cycle the experimental and calculated results were in good agreement, but in this cycle, the process was less efficient with S^S higher in Step B and lower in Step D. For the combined permeate streams, the S^S was 5.37% for Step B and 13.09% for Step D. The loss in process efficiency was directly related with the increasing toluene concentrations over the first three filtrations of this cycle, which led to higher K_S values and, therefore, to higher losses of eutomer through the dissolution mechanism previously described. Notice that, for the second and third filtrations (Figure 4, numbers 2-2 and 2-3), the S^S was actually positive when negative or near zero values are desirable. In other words, a significant elution of eutomer

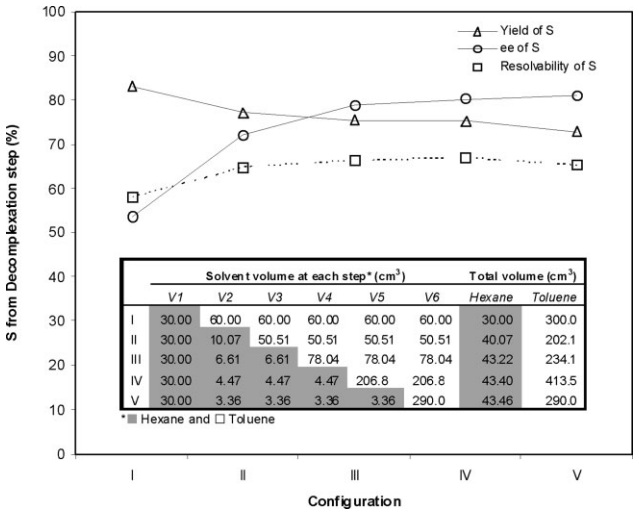

Figure 5. Calculated profiles of resolvability of (*R*)- and (*S*)-PET in combined permeates for the different configurations at optimal feed solvent volumes.

rac-PET at 50 mol/m^3 was employed as substrate and positive *S* indicates (*S*)-rich permeate.

((*S*)-enantiomer) was observed over the (*R*)-elution stage, and inevitably, lower amounts of the eutomer were available for recovery over the (*S*)-elution stage (Step D), leading to lower S^S in Step D (Figure 4, numbers 2-4 to 2-6).

An obvious observation is that, because of the dissolution mechanism, it is important to maintain the toluene concentration at a value much lower than the 20% vol/vol previously established.[9] This can be achieved by using the appropriate number of filtrations in Step E and adding pure *n*-hexane in filtrations within Step B. However, other factors, in addition to higher K_S, such as the feed volume and number of filtrations within Step B, can also promote the dissolution mechanism. Therefore, there is a trade-off in the selection of the number of filtrations and feed volumes in Step B, which are required to achieve an effective elution of distomer and a high process ee, but, which in excess will also prematurely wash off the eutomer into the Step B permeate, leading to lower yields in Step D. Such optimization is the subject of the next section.

Process optimization

The feed solvent volumes were optimized as explained earlier for each of the nanofiltration Configurations I to V (Figure 2). Calculations were performed for *rac*-PET at 50 mol/m^3 using pure *n*-hexane as resolution solvent, and the results were plotted in Figure 5. Similar resolvabilities, as well as yields and ee, were found for the Configurations II to V. Only, Configuration I presented a more moderate resolvability and lower yield and ee. We decided to experimentally operate Configuration II, because it required a lower volume of solvent than the other configurations. Figure 6 provides a schematic summary of the sequence of operations for the optimal Configuration II. Figure 7 shows the resolvabilities for each of the nanofiltration permeates obtained in Steps B and D over one cycle of operations, where calculated and experimental results were in good agreement with an *R*-squared value of 0.993.

The comparison between yield, ee, and S^S of the combined permeate streams of the nonoptimal process (Figure 4) with the ones of the optimal process (Figure 7) are shown in Table 1. It is encouraging to note that the experimental data and the calculated values were in good agreement and exhibit the same trends. As the process was optimized, the resolvability in Step B decreased from -58.0 to -62.0% (experimental values), implying a more selective removal of distomer relatively to the eutomer. The Y^R, and also Y^S, in Step B decreased for the optimal configuration, meaning less eutomer was prematurely washed out of the system, but the respective ee^S also decreased, which implies that a higher quantity of distomer was carried out in Step D. The objective function selected for the optimization was the resolvability in Step D. Therefore, it is obvious that the optimized configuration exhibited an experimental S^S higher than that of the nonoptimal configuration (58.2% vs. 65.2%, experimental values). However, this increase was mainly due to an increase in yield (65.3% vs. 79.4%, experimental values), whereas a decrease in ee was observed (80.1% vs. 69.4%, experimental values). In other words, the resolvability of the final product was increased by performing a weaker elution

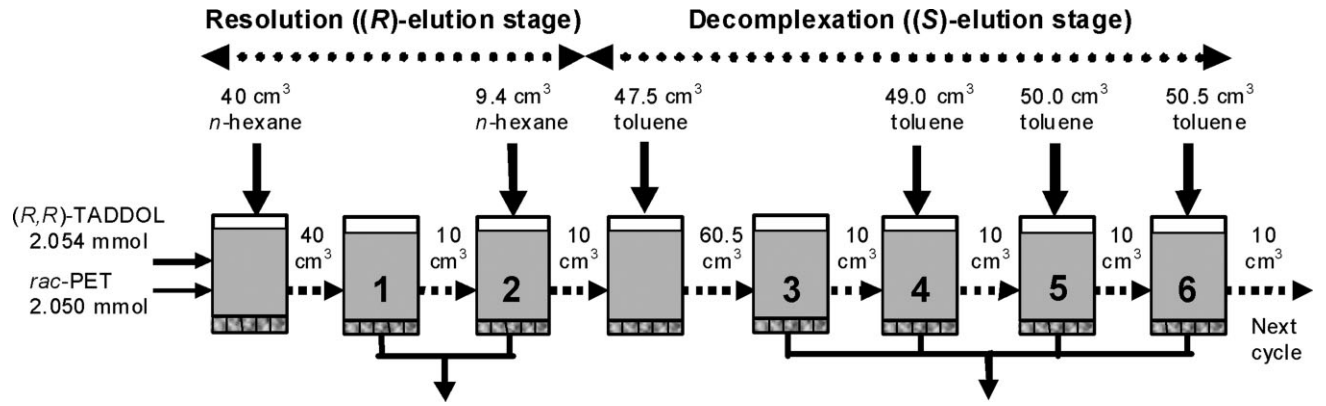

Figure 6. Process schematic summary of EIC-OSN process of 50 mol/m^3 *rac*-PET in equimolar TADDOL at optimal operating conditions of Configuration II.

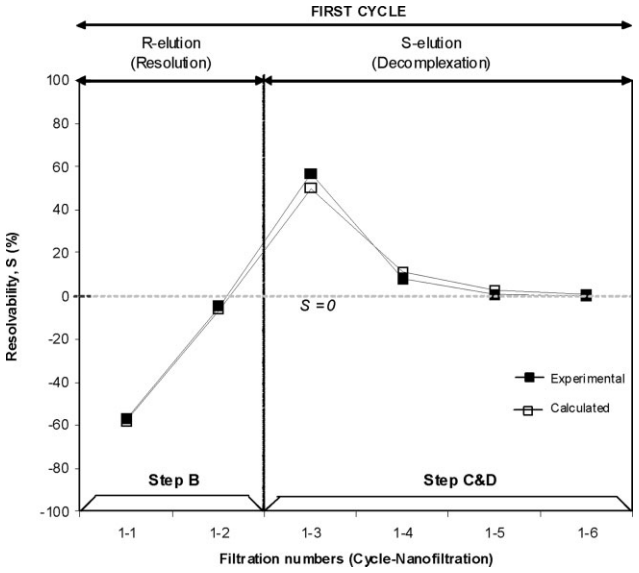

Figure 7. Experimental and calculated profile of (*S*)-PET resolvability (S) for the six nanofiltration permeates at optimal operating conditions of Configuration II.

rac-PET at 50 mol/m^3 was employed as substrate. Positive *S* indicates S-rich permeate. Positive *S* indicates (*S*)-rich permeate. Feed and permeate volumes follow optimal values for configuration II as indicated in Figure 6.

in Step B. This allowed the transfer of higher amounts of the eutomer through the process to permeate of Step D but sacrificed the optical purity of the final product stream.

An alternative strategy could be to impose a constraint on the optical purity of the final stream (permeate of Step D), regardless of the yield obtained. At the operating concentrations, the distomer does not bind to the guest, remaining completely dissolved in the resolution solvent. Hence, before decomplexation takes place in Step C, the distomer can potentially be completely removed from the system by elution during Step B. This would theoretically lead to a 100% eutomer ee in the Step D permeate. However, because an extended elution is performed in Step B (with larger quantities of solvent or higher number of filtrations), the eutomer dissociates to balance the inclusion complex formation equilibrium and is eluted in Step B. Therefore, lower amounts of eutomer reach Step D, leading to lower process yields. The optimization of this resolution process by maximizing resolvability in Step D can lead to a higher ee or yield but not to a simultaneous increase of both of these two variables. This trade off between yield and ee is at the core of the resolution process optimization and can be tailored according to the target application of the process and specific requirements of final product purity.

Figure 8 shows an example where the objective function was still targeting Step D, but maximized yield rather than resolvability with a lower constraint of 85% imposed for the ee^S. Configuration I, with the permeate volume of the first filtration fixed at 30 cm^3, was not able to provide sufficient elution of the distomer in Step B, and consequently, the ee obtained in Step D could not meet the 85% constraint. Configurations II to V met this criterion, and the maximum yield (and resolvability) was achieved by Configuration IV. In this configuration, the optimal permeate/feed volumes for the four filtrations of Step B were relatively low, but it provided an effective removal of distomer, without an excessive loss of eutomer. This suggested that the effectiveness of this step could benefit from a continuous diafiltration. The use of a high volume of decomplexation solvent over the two nanofiltrations of Step D of Configuration IV yielded the required higher elution of the eutomer, which was not achievable with a single nanofiltration for Step D in Configuration V.

Effect of eutomer solubility limits and selection of racemate concentration

As discussed above in the solubilities profiles section, for compounds with lower K_S and higher K_R, it was possible to achieve higher yield, purity, and resolvability of the desired product by selecting a racemate concentration within these two solubility limits. The best results will be obtained when all the eutomer binds with the host (i.e., $K_S = 0$) and all the distomer remains dissolved in solution. This was referred as the best case scenario. The resolvability for this best case scenario, three secondary alcohols and PEA, was calculated at a racemate concentration of 50 mol/m^3. The calculated

Table 1. Comparison of Combined Permeate Yield, ee, and Resolvability of Nonoptimal and Optimal Process

	Y^R (%)		ee^S (%)		S^S (%)	
Data type	Nonoptimal	Optimal	Nonoptimal	Optimal	Nonoptimal	Optimal
(*R*)-PET from Combined (*R*)-Elution Nanofiltration Permeates, Step B						
Experimental	98.5	82.5	−41.8	−60.4	−58.0	−62.0
Calculated	97.5	87.5	−36.1	−58.7	−51.7	−64.7
	Y^S (%)		ee^S (%)		S^S (%)	
Data type	Nonoptimal	Optimal	Nonoptimal	Optimal	Nonoptimal	Optimal
(*S*)-PET from Combined (*S*)-Elution Nanofiltration Permeates, Step D						
Experimental	65.3	79.4	80.1	69.4	58.2	65.2
Calculated	50.5	77.1	91.2	72.2	48.2	64.7

Both experimental data and calculated values are shown.
Positive sign in ee^S and S^S indicates (*S*)-rich permeate.

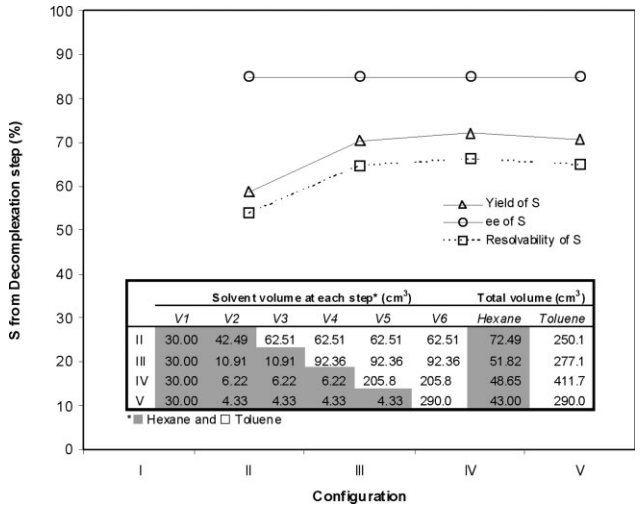

Figure 8. Calculated profiles of (*R*)- and (*S*)-PET in combined permeates for the different configurations at optimal feed solvent volumes.

rac-PET at 50 mol/m^3 was employed as substrate, and positive *S* indicates (*S*)-rich permeate. The purity of (*S*)-PET was set at 85% ee or above (for applicable configuration).

results were summarized in Table 2 and were obtained on the basis of an optimized Configuration II and maximizing the permeate resolvability of Step D. A resolvability of 99.2% was calculated for the best case scenario. As the solubility limit of the eutomer ((*S*)-enantiomer) in *n*-hexane increased, we moved further away from the best case scenario, and more of the eutomer was used to saturate the solution. This was washed out in Step B, leading to a lower yield observed in Step D. From the selected model compounds, the best resolvability was obtained for PET (with K_S = 5.7 mol/m^3), whereas for phenylpropanol, no crystalline inclusion complex was formed, because at a racemate concentration of 50 mol/m^3, there was insufficient (*S*)-enantiomer to saturate the *n*-hexane solution (K_S = 25 mol/m^3). In this latter case, the resolution required the use of higher concentrations of racemate and host.

Interestingly, despite PET having similar organic structure to PEA (i.e., the difference is between the hydroxyl group and the amine group), their K_S values are significantly different. From the inspection of the X-ray crystal structures of inclusion complexes of both compounds, the interactions between (*S*)-PET-TADDOL and (*S*)-PEA-TADDOL were almost identical.[9,11] The higher K_S, observed for PEA, must then result from the only difference between the two crystalline structures, which is the strength of the hydrogen bond between "O" in PET and "N" in PEA. Such difference is related to a higher electronegativity of the oxygen than the nitrogen atom (i.e., 3.44 and 3.04, respectively).[12] The stronger this bond, the lower the complex energy, shifting the equilibrium of the complexation reaction toward the formation of the complex, and subsequently, less amount of (*S*)-enantiomer is required to saturate the mother liquor.

It is also interesting to note from the experimental data that the smaller the racemic secondary alcohols, the better the enantioselectivity of inclusion (i.e., lower K_S). This can be explained by the nature of the complexation mechanism with (*R,R*)-TADDOL. The larger groups in the guest seem to open up the square of hydrogen bonds between two host molecules that forms the 2:1 host-eutomer inclusion complex. In other words, the compound with higher molecular weight, when accommodated by the host molecules, forms less energetically stable complexes, requiring higher amount of (*S*)-enantiomer in the mother liquor.

Because of practical reasons, the experimental work and the model calculations were performed at 50 mol/m^3. However, the process could benefit from using different concentrations. Figure 3 shows that (*S*)-enantiomer solubility limit was concentration dependent, with a slight increase of K_S as the racemate concentration increased (the TADDOL: racemate equimolar ratio is maintained). However, the trend for the solubility limit followed a relatively low slope and had a high intercept with the "y" axis. Thus, the higher the substrate and guest concentrations, the larger the fraction of the feed eutomer ((*S*)-enantiomer) was used to form the inclusion complex. Therefore, higher yields and optical purities could be achieved by working at higher feed concentrations as long as the distomer ((*R*)-enantiomer) concentration remained below its solubility limit (Figure 3), avoiding decreases in the ee. On the other hand, as higher racemate and TADDOL concentrations were used, the resulting *n*-hexane solution became increasingly viscous due to the solid crystalline inclusion complex, making it difficult to mix and nanofilter the solution in Step B. This drawback might be overcome by a system in which Step B would comprise a different separation system of solids such as microfiltration or centrifugation.

The idea of using higher feed concentrations was theoretically explored for PET, calculating the resolvability obtained as a function of *rac*-PET initial concentrations, in a range of 25 to 400 mol/m^3. These calculations were performed on the basis of Configuration II at the optimal conditions, and the

Table 2. Process Performance for Resolution of Various Secondary Alcohols and Amine Racemates Solution in *n*-Hexane at 50 mol/m^3 Feed Concentrations (Calculations Based on Configuration II as Described in Figure 6), Compared With Hypothetical Best Case (K_S = 0)

			Step B ((*R*)-elution)			Step D ((*S*)-elution)		
Compound	K_S (mol/m^3)	MW (g/mol)	Yield (%)	ee (%)	S_R^S(%)	Yield (%)	ee (%)	S_D^S(%)
Best Case	0.0	–	99.2	100	−99.2	100.0	98.4	99.2
Phenylethanol	5.7	122.17	87.5	58.7	−64.7	77.1	72.2	64.7
Phenylpropargyl alcohol	6.7	132.16	87.6	53.2	−60.8	73.3	71.0	60.8
Phenylethylamine	18.9	121.18	78.5	13.5	−18.7	40.2	30.2	18.7
Phenylpropanol	25.0	136.20	93.8	0.0	0.0	6.2	0.0	0.0

Positive *S* indicates (*S*)-rich permeate and the calculation based on equimolar TADDOL host and Configuration II.

Table 3. Process Performance for Resolution of *rac*-PET in *n*-Hexane at Various Feed Concentrations (Calculations Based on Configuration II as Described in Figure 6)

Concentration (mol/m^3)	K_S (mol/m^3)	Step B ((*R*)-elution)				Step D ((*S*)-elution)		
		Yield (%)	ee (%)	S_R^S(%)	S loss (%)	Yield (%)	ee (%)	S_D^S(%)
25	5.6	82.8	36.1	−44.0	38.8	61.1	56.1	44.0
50	5.7	87.5	58.7	−64.7	22.8	77.1	72.2	64.7
100	7.5	90.1	68.2	−73.1	17.0	82.9	78.6	73.0
200	10.1	92.3	74.9	−79.1	13.2	86.7	83.7	79.0
400	15.2	93.2	79.3	−82.4	10.8	89.2	85.9	82.4

Positive *S* indicates (*S*)-rich permeate and the calculation based on equimolar TADDOL host and Configuration II.

results obtained are summarized in Table 3. As expected, for higher feed concentrations, lower fractions of eutomer were lost in the distomer elution stage (Step B), and so the resolvability of the eutomer in Step D increased by 40% as the feed concentration increased from 25 to 400 mol/m^3. The same trend was observed in the calculations for the other racemates (Table 4), with dramatic improvements of the resolvability of Step D for a concentration of 400 mol/m^3. This is illustrated by the cases of phenylpropargyl alcohol and phenylpropanol, which were not resolved at 50 mol/m^3, or the case of PEA, for which resolvability increased from only 18.7% to an interesting value of 73.3%. In principle, operation at higher concentrations could be executed if the physical limitations are overcome.

Effect of distomer solubility limits

For all substrates selected on this study, there is no significant binding between distomer and host at the concentrations tested (Figure 3a), and therefore the assumption that only the eutomer binds to the host holds for such cases (assumption c). However, there maybe other cases wherein such assumptions are no longer valid.

In the case where the distomer does not remain completely dissolved throughout the entire process, both mechanisms, dissolution (for resolution) and dilution (for decomplexation), are applied. Therefore, Eqs. 7 and 8 are replaced by Eqs. 12 and 13:

$$M_n^R = V_{P,n} K_R \qquad for\ n\ =\ 1, 2, 3, ..., d \tag{12}$$

$$M_n^R = \frac{V_{P,n}}{V_{F,n}} \left(M_o^R - \sum_{i=1}^{n-1} M_i^R \right) \quad for\ n\ =\ d+1,\ d+2,\ d+3, ... \tag{13}$$

To illustrate the effect of selectivity of TADDOLs, different solubilities for the distomer (K_R) were applied. Calculations were performed for a nonoptimal process with a single resolution and decomplexation stage using Configuration III, with a volume of permeate, and the corresponding solvent addition fixed at 30 cm^3 in every nanofiltration. The feed was a 40 cm^3 solution with a racemate concentration of 50 mol/m^3. The eutomer solubility was assumed to be the same as (*S*)-PET (5.7 mol/m^3), the distomer solubilities were varied from 5.7 to 8, 10, and >50 mol/m^3. The first case ($K_R = K_S$) implied no discrimination of the host between eutomer and distomer, and the last case (K_R > feed concentration) is the previously discussed case where no binding between host and distomer is observed.

The results presented in Table 5 show a dramatic impact on the process resolvability at the lower resolution selectivity where more distomer binds to the host.

Batch multistage process

As discussed above, the final product purity (i.e., ee in the combined permeates of Step D) could be improved by increasing the extension of elution during Step B ((*R*)-elution), permeating larger volumes of *n*-hexane in each filtration and/or using additional nanofiltrations. However, this strategy would also contribute to increasing losses of eutomer through permeate in Step B due to the dissolution mechanism. The calculations in Table 3 indicate a clear improvement in eutomer resolvability when higher feed concentrations were employed in the resolution (Step A), because a lower fraction of the feed eutomer was washed out together with the distomer in Step B. However, notice that, despite a larger fraction of the feed eutomer being isolated in Step D, this process improvement was actually accompanied by an increase in losses of absolute amounts of the eutomer

Table 4. Comparison Between Process Performance for Various Secondary Alcohols and Amine Racemates Solution in *n*-Hexane at Feed Concentration of 50 and 400 mol/m^3 (Calculations Based on Configuration II as Described in Figure 6), Compared With Hypothetical Best Case (K_S = 0)

Compound	MW (g/mol)	Step D ((*S*)-elution)							
		Feed: 50 mol/m^3				Feed: 400 mol/m^3			
		K_S (mol/m^3)	Yield (%)	ee (%)	S_D^S(%)	K_S (mol/m^3)	Yield (%)	ee (%)	S_D^S(%)
Best Case	–	0.0	100.0	98.4	99.2	0.0	100.0	98.4	99.2
Phenylethanol	122.17	5.7	77.1	72.2	64.7	15.2	89.2	85.9	82.4
Phenylpropargyl alcohol	132.16	6.7	73.3	71.0	60.8	8.7*	83.3*	79.2*	73.7*
Phenylethylamine	121.18	18.9	40.2	30.2	18.7	29.7	83.1	78.8	73.3
Phenylpropanol	136.20	25.0	6.2	0.0	0.0	75.8	66.1	61.3	50.3

Positive *S* indicates (*S*)-rich permeate and the calculation based on equimolar TADDOL host and Configuration II.
*Because the racemate solubility limit in *n*-hexane is 130.6 mol/m^3, calculations for this guest were performed at 120 mol/m^3, instead of 400 mol/m^3.

Table 5. Comparison Between Process Performance for Various Distomer Solubilities (Calculations Based on Nonoptimal Configuration III With Feed Concentration of 50 mol/m^3 and Eutomer Solubility of 5.7 mol/m^3)

		Step B ((*R*)-elution)			Step D ((*S*)-elution)		
K_R (mol/m^3)	K_S (mol/m^3)	Yield (%)	ee (%)	S_R^S(%)	Yield (%)	ee (%)	S_D^S(%)
5.7	5.7	51.2	0.0	0.0	48.0	0.0	0.0
8	5.7	72.0	16.9	−20.8	48.0	27.1	20.5
10	5.7	90.0	27.5	−38.8	48.0	66.0	38.2
>50	5.7	98.4	31.6	−47.2	48.0	93.8	46.5

Positive *S* indicates (*S*)-rich permeate and the calculation based on equimolar TADDOL host and Configuration III.

through the permeate of Step B as K_S increased with concentration. Therefore, the performance of this process could be further improved by a multistage filtration in which a secondary process (Figure 9, process 1b) was added with the aim of recovery of eutomer from the Step B permeate of the primary process (Figure 9, process 1a).

In the multistage process, the Step B permeate arising from the primary process (Figure 9, stream 2) was used as feed of Step A of the secondary process. The scope for additional improvement in resolution performance using this multistage process relied on the difference between the substrate concentrations in the primary and secondary processes. The primary process was fed (Figure 9, stream 1) with a higher eutomer concentration than the secondary stage, and therefore the respective solubility limits were also different (e.g., a K_S of 15.2 and 5.7 mol/m^3 for a 400 and 50 mol/m^3 *rac*-PET concentrations, respectively).

To illustrate the multistage process, calculations were performed for a nonoptimal process, where *rac*-PET was fed at 400 mol/m^3 (16 mmol) in *n*-hexane to the primary process. Calculations were performed assuming that the primary process was carried out in configuration III with a volume of permeate, and the corresponding solvent addition fixed at 30 cm^3 in every nanofiltration. Step B of the primary process (process 1a) yielded a combined permeate stream rich in distomer (stream 2), but still with significant amounts of the eutomer, (*S*)-enantiomer (1.37 mmol, 17% of the eutomer in stream 1). This stream was fed for additional resolution into the secondary process, for which calculations were performed assuming configuration II, but with the concentrations of 87.5 and 15.2 mol/m^3 for eutomer and distomer, respectively, instead of the concentrations of 25 mol/m^3 for each of the enantiomers reported in Figure 6. The model calculated a stream 7 with 0.74 mmol of eutomer and 0.22 mmol of distomer, which implied a recovery of about half of the eutomer fed to the secondary process in stream 2. The combination of all the permeates from the Steps D from primary and secondary processes (streams 3, 7, and 11 from process 1a and 1b) had a S^S of 86.6%, whereas the S^S in the Step D of the primary process alone was 80.1%. This enhancement in resolvability was achieved through the improvement in yield (Y_D^S of 90.9% and 81.6% for the multistage and primary process alone, respectively) and sacrificed optical purity (ee_D^S of 91.1% and 96.4% for the multistage and primary process alone, respectively). Whether this gain in process performance makes it worthwhile to add the secondary process or if the slight losses of optical purity become prejudicial has to be assessed on the basis of the specific application target and final product specifications.

Notice also that Stream 2 comprised a volume 90 cm^3 instead of the usually 40 cm^3 used in the resolution of Step A. This volume was relatively large and could be reduced by further optimizations. Furthermore, *n*-hexane has a boiling point of 69°C, and therefore solute concentrations in Stream 2 could be increased by evaporation of the solvent as long as the concentration of the distomer does not become higher than its solubility. Any of the strategies adopted to obtain higher solute concentrations in Stream 2 would result in a higher feed concentration of the secondary process, enhancing the respective resolution efficiency.

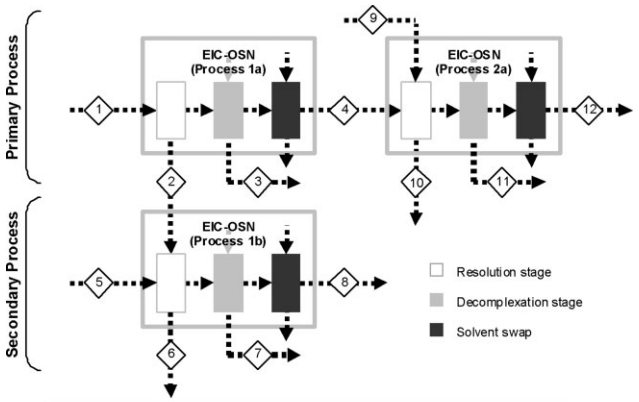

Stream Description			
Stream	Details	Stream	Details
1	*rac*-PET and TADDOL	7	(*S*)-rich permeate (Product)
2	(*R*)-rich permeate	8	Hexane-rich solvent*
3	(*S*)-rich permeate (Product)	9	Host and guest makeup
4	Hexane-rich solvent	10	(*R*)-rich permeate*
5	Host and solvent makeup	11	(*S*)-rich permeate (Product)
6	(*R*)-rich permeate (Product)*	12	Hexane-rich solvent*

*Feed to further filtration process (if any)

Figure 9. Multistage EIC-OSN process diagram of 400 mol/m^3 *rac*-PET with excess (*R,R*)-TADDOL.

Configuration III was employed in Process 1a and 2a while Configuration II was employed in Process 1b.

Conclusions

In this article, the EIC-OSN process was mathematically designed and developed. The model equations use the combination of fundamental mass balances, solubility of inclusion complex, and rejection of enantiomers and take into account the two filtration mechanisms: dissolution and dilution. The comparison of the model with experiments shows good agreement with calculated data. Based on the validated model, optimization over the solvent addition step and added solvent volume was performed. The optimal results show a better separation performance represented by an increase in resolvability to more than 60%. The calculations show that depending on the objective function selected, e.g.,

resolvability versus yield with a constraint on product optical purity, different configurations are optimal. This suggests that further investigations towards the use of a diafiltration in Step B may be interesting. The studies of the effects of solubility of the inclusion complex and feed concentration show that lower eutomer solubility and higher feed concentration are desirable. However, further experimental work is required to perform the process at higher concentrations, where increases in viscosity and suspended solids pose additional filtration challenges. This work also proposes a multistage EIC-OSN process, in which a combination of higher feed concentrations and recovery of the eutomer in a secondary process can provide further increases in resolvability of the overall process. For the four selected racemates, there is no significant binding between host and distomer. However, the application of the present process could become more challenging when higher amounts of distomer binds to the host resulting in lower process resolvability.

Acknowledgments

NFG acknowledges financial support from the Ministry of Science, Technology and Innovation (MOSTI) of Malaysia. FCF acknowledges financial support from Fundação para a Ciência e Tecnologia (SFRH/BPD/19369/2004). Special thanks to Xun Xing Loh and Ines Baptista for their input in preparation of this article.

Notation

d = step number of last resolution of a particular cycle
ee = enantiomeric excess, %
ee_n^R = enantiomeric excess of (*R*)-enantiomer corresponding to yield at step *n*, %
ee_n^S = enantiomeric excess of (*S*)-enantiomer corresponding to yield at step *n*, %
K_R = saturation concentration of complexed (*R*)-enantiomer, distomer, mol/m^3 or mmol/m^3
K_S = saturation concentration of complexed (*S*)-enantiomer, eutomer, mol/m^3 or mmol/m^3
M_o = initial moles of racemate fed to the cycle, mmol
M_o^R = initial moles of (*R*)-enantiomer fed to the cycle, mmol
M_o^S = initial moles of (*S*)-enantiomer fed to the cycle, mmol
M_n^R = number of moles of permeated (*R*)-enantiomer at step *n*, mmol
M_n^S = number of moles of permeated (*S*)-enantiomer at step *n*, mmol
n = step number
rac = racemic
S = resolvability, %
S_D^S = combined resolvability of (*S*)-enantiomer from decomplexation stage (i.e., (*S*)-elution stage), %
S_n^R = resolvability of (*R*)-enantiomer at step *n*, %
S_n^S = resolvability of (*S*)-enantiomer at step *n*, %
S_R^R = combined resolvability of (*R*)-enantiomer from resolution stage (i.e., (*R*)-elution stage), %
$V_{F,n}$ = initial volume of feed at step *n*, cm^3
$V_{P,n}$ = volume of permeate from step *n*, cm^3
Y_n^R = (*R*)-enantiomer yield of permeate from step *n*, %
Y_n^S = (*S*)-enantiomer yield of permeate from step *n*, %

Greak letter

γ_i^l = activity coefficient of liquid phase

Literature Cited

1. Breuer M, Ditrich K, Habicher T, Hauer B, Kesseler M, Stürmer R, Zelinski T. Industrial methods for the production of optically active intermediates. *Angew Chem Int Ed*. 2004;43:788–824.
2. Kozma D. *CRC Handbook of Optical Resolution via Diastereomeric Salt Formation*. Boca Raton: CRC Press, 2002.
3. Toda F. Inclusion by acetylenic alcohols and some other novel host compounds. In: Atwood JL, Davies JED, MacNicol DD. *Inclusion compounds: Volume 4*. New York, NY: Oxford University Press, 1991:126–187.
4. Pellissier H. Use of TADDOLs and their derivatives in asymmetric synthesis. *Tetrahedron*. 2008;64:10279–10317.
5. Müller S, Afraz MC, de Gelder R, Ariaans GJA, Kaptein B, Broxterman QB, Bruggink A. Design and evaluation of inclusion resolution, based on readily available host compounds. *Eur J Org Chem*. 2005;1082–1096.
6. Xie R, Chu L-Y, Deng J-G. Membranes and membrane processes for chiral resolution. *Chem Soc Rev*. 2008;37:1243–1263.
7. Vandezande P, Gevers LEM, Vankelecom IFJ. Solvent resistant nanofiltration: separating on a molecular level. *Chem Soc Rev*. 2008;37:365–405.
8. Nasso M, Livingston AG. Solvent nanofiltration in organic process: a rapid and scalable purification technology. *Chim Oggi*. 2008;26:62–66.
9. Ghazali NF, Ferreira FC, White AJP, Livingston AG. Enantiomer separation by enantioselective inclusion complexation-organic solvent nanofiltration. *Tetrahedron Asymmetry*. 2006;17:1846–1852.
10. Fogassy E, Lopata A, Faigl F, Darvas F, Ács M, Tõke L. A quantitative approach to optical resolution. *Tetrahedron Lett*. 1980;21:647–650.
11. Toda F, Tanaka K, Ootani M, Hayashi A, Miyahara I, Hirotsu K. Structure study of host-guest molecular association in solution and in the solid state. *J Chem Soc Chem Commun*. 1993;1413–1415.
12. Allred AL. Electronegativity values from thermochemical data. *J Inorg Nucl Chem*. 1961;17:215–221.

Manuscript received Aug. 8, 2008, and revision received Jun. 26, 2009.